

Time-resolved structural analysis of K- and Ba-exchange reactions with synthetic Na-birnessite using synchrotron X-ray diffraction

CHRISTINA L. LOPANO,^{1,*} PETER J. HEANEY,¹ JEFFREY E. POST,² JONATHAN HANSON,³ AND SRIDHAR KOMARNENI⁴

¹Department of Geosciences, Penn State University, University Park, Pennsylvania 16802, U.S.A.

²Department of Mineral Sciences, Smithsonian NMNH, Washington, D.C. 20013-7012, U.S.A.

³Department of Chemistry, Brookhaven National Lab, Upton, New York 11973, U.S.A.

⁴Department of Crop and Soil Sciences and Materials Research Institute, Penn State University, University Park, Pennsylvania 16802, U.S.A.

ABSTRACT

Time-resolved Rietveld refinements using synchrotron X-ray diffraction (XRD) have documented real-time changes in unit-cell parameters in response to cation substitution in synthetic Na-birnessite. Potassium- and Ba-birnessite, like Na-birnessite, were found to have triclinic symmetry. Rietveld analyses of the XRD patterns for K- and Ba-exchanged birnessite revealed decreases in the *a*, *c*, and β unit-cell parameters, with a decrease of 1.7 and 0.5%, respectively, in unit-cell volume relative to Na-birnessite. Fourier electron difference syntheses revealed that the changes in the configuration of the interlayer species, and the charge, size, and hydration of the substituting cations, serve as the primary controls on changes in unit-cell parameters. Split electron density maxima with centers at (0 0 0.5) were present for Na, K, and Ba end-members; however, with increased substitution of K⁺ for Na⁺, the axis connecting the split-site maxima rotated from an orientation parallel to the *b*-axis to along the *a*-axis. Substitution of Ba²⁺ for Na⁺ did not result in rotation, but splitting of the interlayer site was more pronounced.

Keywords: Birnessite, cation exchange, synchrotron, X-ray diffraction, Mn-oxide

INTRODUCTION

Birnessite is one of the most common Mn oxides found in nature. Manganese oxides having the birnessite-type layer structure occur as fine-grained aggregates, veins, marine and freshwater nodules and concretions, crusts, dendrites, and coatings on other mineral particles and rock surfaces (Burns and Burns 1976; Dixon et al. 1986; Cornell and Giovanoli 1988; Post 1992, 1999). As a result of their fine grain sizes, birnessite phases have large surface areas for cation-exchange and redox reactions; therefore, even small amounts can significantly influence the chemical compositions of sediments and aqueous systems with which they are in contact (Paterson et al. 1986; Golden et al. 1986, 1987; Banerjee and Nesbitt 1999). The unusually high adsorption capacities and scavenging capabilities of Mn oxide/hydroxide minerals make their presence in soils a primary control on heavy metal and trace-element mobility; these characteristics make them useful geochemical exploration tools and water purification agents (Post 1999). Synthetic birnessite-like phases are extensively studied for use as catalysts, cation-exchange agents, octahedral sieves, and battery materials (Shen et al. 1993; Luo et al. 1998; Feng et al. 1999; Leroux et al. 2001). However, the same fine-grained texture that makes birnessite so reactive also makes its crystal structure difficult to study since crystals are generally unsuitable for single-crystal diffraction.

Birnessite is a layered Mn oxide consisting of edge-sharing Mn-O octahedra with an ~ 7 Å basal spacing (Fig. 1). The inter-

layer region of natural birnessites is occupied by hydrated cations, such as Na⁺, Ca²⁺, and K⁺. Since birnessite readily exchanges these interlayer cations, a variety of birnessite-type structures can be synthesized with different cations in the interlayer. Despite the plethora of synthesis methods for birnessite (McKenzie 1971; Golden et al. 1986; Shen et al. 1993; Luo and Suib 1997; Feng et al. 1999; Ma et al. 1999; Luo et al. 2000), details concerning the changes in atomic structure associated with cation exchange are not well documented. Because of the poorly crystalline nature of natural birnessite, structure refinement by powder diffraction is difficult, and synthetic birnessite typically is studied as an analog to the natural material (Kuma et al. 1994).

Recent studies have reported refinements of the structure of Na-birnessite using synchrotron powder XRD coupled with Rietveld analysis. This work has revealed that Na-birnessite is triclinic (Post et al. 2002; Lanson et al. 2002), not monoclinic, as was previously believed (Post and Veblen 1990). In the present study, we used synchrotron radiation, imaging plate technology, and a flow-through capillary cell (Parise et al. 2000; Lee et al. 1998, 2000) to monitor in real-time structural changes as dissolved K⁺ and Ba²⁺ exchanged for Na⁺ in the interlayer of birnessite. The crystal structures of the K- and Ba-birnessite end-members, as well as the intermediate, partially exchanged phases, were determined using Rietveld analysis with the same methods described by Post et al. (2002). The purpose of our study was to provide a more complete understanding of the way in which birnessite incorporates metal cations into its crystal structure. Insights into this exchange process will assist in the development of birnessite-type phases as catalysts and cation-exchange agents, and they will provide

* E-mail: clopano@geosc.psu.edu

a deeper understanding of the geochemical role of birnessite in natural systems.

EXPERIMENTAL METHODS

Sample preparation

The Na-birnessite samples used in the Ba-exchange experiments were derived from the same synthetic batch used by Post and Veblen (1990) and Post et al. (2002), with the formula $\text{Na}_{0.58}(\text{Mn}_{1.42}^{4+}, \text{Mn}_{0.58}^{3+})\text{O}_4 \cdot 1.5\text{H}_2\text{O}$. This material contained a small quantity of hausmannite (~5 wt%). Examination by transmission electron microscopy revealed that the crystals were plate-like and measured ~1 μm across and several hundred Ångströms thick (Post and Veblen 1990). The Na-birnessite samples used in the K-exchange were freshly synthesized using the same methods employed by Post and Veblen (based on protocols in Golden et al. 1986, 1987). A solution of NaOH (55 g of NaOH in 250 mL of H_2O) was added to 200 mL of a chilled 0.5 M MnCl_2 solution and reacted at room temperature while oxygen was bubbled through the $\text{Mn}(\text{OH})_2$ suspension at a rate of ≥ 1.5 L/min through a glass frit. Similar to the procedure outlined in Kuma et al. (1994), the precipitate was filtered through a 0.1 μm Millipore filter, washed, and stored as a suspension until aliquots were removed and air-dried for use. XRD patterns of the initial Na-birnessite samples used in the K-exchange reactions revealed no evidence of significant amounts of hausmannite (<1%).

Data collection

XRD data were collected at beam line X7B of the National Synchrotron Light Source (NSLS), Brookhaven National Laboratory (BNL), with an X-ray wavelength of 0.9044 Å (as determined from a LaB_6 standard) for the K- and Ba-exchange. A small amount (~1 mg) of birnessite was loaded into 0.5 or 0.7 mm quartz capillaries and held in place by cotton or glass wool on either side of the sample. The capillary was inserted into a flow-through apparatus similar to the SECR $\bar{\text{e}}$ TS (Small Environmental Cell for Real-Time Studies) cell described by Parise et al. (2000) for the exchange reactions used in studies by Lee et al. (1998, 2000). XRD patterns were collected every 2 to 3 minutes with a MAR345 full-imaging plate detector for periods of 1 to 4 hours as 0.01 M solutions of KCl or BaCl_2 at neutral pH flowed through the sample (on average 1 drop/100 s) under N_2 pressure. During exposure, the sample was rotated through a 10° phi angle. Preferred orientation of the powder was eliminated through a combination of specimen rotation, use of a capillary sample holder, and full intensity integration of the diffraction rings, as obtained using the program FIT2D (Hammersley et al. 1996) with a polarization factor of 0.93. The series of time-resolved XRD patterns collected during the K-exchange and Ba-exchange reactions can be seen in Figures 2 and 3, respectively.

The exchanged samples were placed on a carbon stub and analyzed using

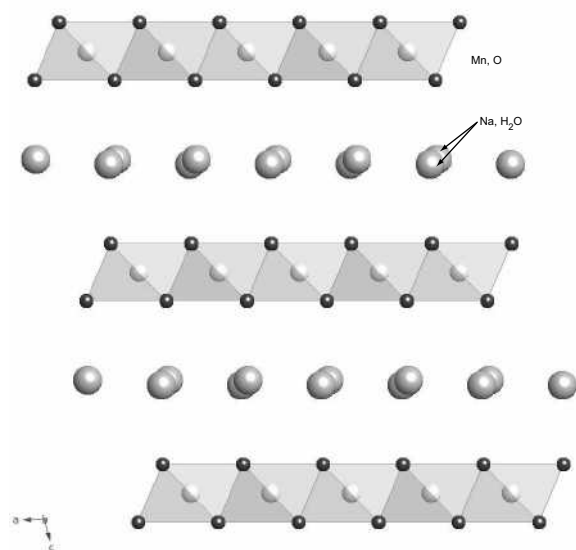


FIGURE 1. View of the synthetic Na-birnessite [$\text{Na}_{0.58}(\text{Mn}_{1.25}^{4+}, \text{Mn}_{0.58}^{3+})\text{O}_4 \cdot 1.5\text{H}_2\text{O}$] structure approximately along the b axis.

energy dispersive X-ray spectroscopy (EDS), with a JEOL JSM-840A scanning electron microscope (SEM) and an attached Noran System dispersive X-ray analyzer. The results indicated that both the K-exchanged samples were completely exchanged and the Ba-exchanged samples contained little to no Na^+ (~1 wt%) by the completion of the experimental runs. The small sample size and the fine-grained powdered nature prevented accurate quantitative chemical analysis by electron-beam methods. Chemical analyses of the starting Na-birnessite material can be found in Post and Veblen (1990).

Structure refinement

Rietveld structure refinements (Rietveld 1969) were performed using the EXPGUI interface (Toby 2001) of the General Structure Analysis System (GSAS) developed by Larson and Von Dreele (2006). The initial structure parameters for the starting Na-birnessite material came from the triclinic structure of Post et al. (2002). The latter authors employed triclinic rather than monoclinic symmetry on the basis of split diffraction peaks (such as the 011, 101, 102), as was revealed by synchrotron XRD. We observed that these peaks also were split in our K- and Ba-birnessite patterns, indicating that these structures are triclinic as well.

For the calculation of Fourier electron difference maps, the interlayer species were excluded. The backgrounds for the XRD patterns were fit using up to 28 terms for Na-, K-, and Ba-birnessite, with a linear interpolation function. The peak profiles were modeled by a pseudo-Voigt profile function as parameterized by Thompson et al. (1987), with asymmetry corrections by Finger et al. (1994) and microstrain anisotropic broadening terms by Stephens (1999). During initial cycles of refinement, only the background, scale, peak profile, and unit-cell parameters were allowed to vary. The position of the O atom in the Mn-O sheet was then refined. Calculations of difference electron Fourier (DELF) maps were performed to determine the interlayer atom positions. Once located, the interlayer atoms were added to the refinement as a single O_{int} site, which served to model the average combined water and cation sites. As discussed below, for the completely exchanged phases, the O_{int} site was replaced with separate cation and O sites. Following refinements of the interlayer atom positions, occupancy factors and isotropic atomic displacement factors for the interlayer site were allowed to vary. During the K-birnessite refinement, soft constraints were applied to the Mn-O distances (constrained to 1.85 Å with a standard deviation of 0.03 Å), and the weighting factor was gradually reduced in successive cycles until it was eventually eliminated.

RESULTS AND DISCUSSION

Effects of cation substitution on lattice parameters

The exchange of interlayer cations in birnessite resulted in variations in diffraction peak intensities and positions with increasing degree of exchange (Figs. 2 and 3). Specifically, replacement of Na by K resulted in gradually decreasing intensity of certain peaks (e.g., 001, 111, and 111), shifting of peaks (e.g., 202 and 200), and merging of peaks (e.g., 202 with 111). Barium exchange yielded an abrupt decrease in all peak intensities and abrupt peak shifts (e.g., the 202 and 004 peaks). The final refinement parameters are listed in Table 1. Atomic positions can be found in Table 2 with the corresponding bond distances in Table 3.

The final end-member diffraction patterns of K- and Ba-birnessite showed significant decreases in peak-to-background ratios in comparison with that of the initially dry Na-birnessite material (Fig. 4), most likely due to the increased background caused by the presence of water. Rietveld analyses of XRD patterns obtained at intervals of approximately 5 minutes revealed strong dependencies of the unit-cell parameters with time (Figs. 5 and 6). The error bars for Figures 5 and 6 are smaller than the plotted data symbols. The standard deviations calculated by GSAS for the lattice parameters typically are smaller than the true errors (Post and Bish 1989), and we present the errors calculated by GSAS in the tables and figures of this paper with the understanding that the actual errors may be more than an order

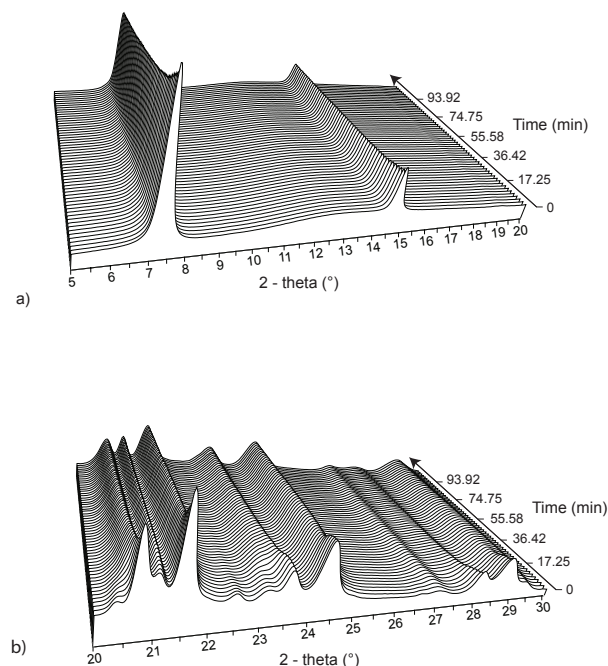


FIGURE 2. Series of XRD patterns showing changes in peak positions and intensities during exchange of K for Na in the birnessite interlayer: (a) 5–20 °2θ; (b) 20–30 °2θ. Each line represents about 2 minutes in time.

TABLE 1. Final Rietveld refinement parameters for Na-, K-, and Ba-birnessite

	Na-birnessite	K-birnessite	Ba-birnessite
Space group	$C\bar{1}$	$C\bar{1}$	$C\bar{1}$
Unit cell			
a (Å)	5.1780(8)	5.1371(5)	5.1713(5)
b (Å)	2.8509(6)	2.8476(2)	2.8473(9)
c (Å)	7.3344(9)	7.2129(8)	7.3039(6)
α (°)	89.45(4)	89.95(1)	89.533(8)
β (°)	103.18(9)	100.74(7)	102.968(3)
γ (°)	89.91(1)	89.704(9)	89.903(7)
V (Å ³)	105.41(4)	103.66(4)	104.802(7)
Refinement			
No. of diffraction points	2519	2470	2552
No. of reflections	307*	167	273*
Diffraction Range (2θ)	4.0–55.99	4.085–58.385	4.0–55.99
No. of variables	97*	60	114*
$R(F^2)$	0.019	0.042	0.034
R_{wp}	0.016	0.020	0.017
χ^2	1.77	1.81	1.41

* Contain small hausmannite impurities.

of magnitude higher than the calculated deviations. During the exchange of K and Ba for Na, the a , c , and β unit-cell parameters decreased, with an overall unit-cell volume contraction of 1.7% for K-exchange and 0.5% for Ba-exchange, relative to Na-birnessite (Figs. 5 and 6). The refined unit-cell volume of the starting Na-birnessite for the K-exchange reactions was slightly lower than the refined unit-cell volumes for Na-birnessite in our other experiments (104.92 vs. 105.41 Å³). We infer that a small degree of exchange already had begun before the first diffraction pattern was collected.

TABLE 2. Atomic coordinates and isotropic displacement factors for Na-, K-, and Ba-birnessite

	Atom	x	y	z	Site occupancy factor	$U_{iso} \times 10^2$ (Å ²)
Na-birnessite	Mn	0	0	0	1.0	0.45(6)
	O	0.3686(3)	-0.0241(2)	0.1307(4)	1.0	1.38(3)
	O _{int}	-0.0270(5)	0.3154(5)	0.4885(4)	0.3453	7.26(1)
	Na	-0.0270(5)	0.3154(5)	0.4885(4)	0.145†	7.26(1)
K-birnessite	Mn	0	0	0	1.0	0.58(8)
	O	0.3717(4)	0.0331(1)	0.1348(0)	1.0	3.18(0)
	O _{int}	-0.1835(6)	0.6099(4)	0.4931(1)	0.388(6)	6.73(2)
	K	-0.1835(6)	0.6099(4)	0.4931(1)	0.115†	6.73(2)
Ba-birnessite	Mn	0	0	0	1.0	0.18(3)
	O	0.3777(5)	-0.0301(5)	0.1321(6)	1.0	1.70(2)
	O _{int}	0.5830(6)	0.2093(7)	0.5069(1)	0.222(2)	10.00*
	Ba	0.5830(6)	0.2093(7)	0.5069(1)	0.0725†	10.00*

* Fixed.

† Determined from analytical data in Post and Veblen (1990).

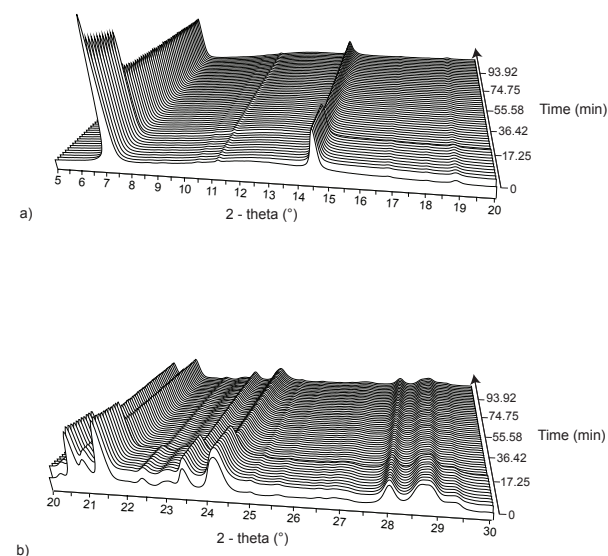


FIGURE 3. Series of XRD patterns showing changes in peak positions and intensities during exchange of Ba for Na in the birnessite interlayer over time: (a) 5–20 °2θ; (b) 20–30 °2θ. Each line represents about 2 minutes in time.

Kuma et al. (1994) argue that the unit-cell parameters of birnessite are a function of the ionic radii, charge, and hydration radii of the interlayer cations. We observed that the decreases in a , c , β , and cell volume with increasing exchange were more pronounced when K⁺ substituted for Na⁺ in comparison with Ba²⁺. This behavior may be attributed to differences in the ionic charge and hydration state of the two cations. K⁺ has an ionic radius of 1.52 Å (Shannon 1976) and a hydration radius of 3.3 Å (Nightingale 1959). Although Na⁺ has a smaller ionic radius (1.16 Å) (Shannon 1976), its hydration radius of 3.6 Å is larger than that of K⁺ (Nightingale 1959). Because these cations are coordinated primarily by water molecules (in this case, six) within the interlayer and two O atoms in the Mn-O sheet of birnessite, the smaller hydration radius for K⁺ induced a small unit-cell contraction of the interlayer region, as reflected in decreases in a , c , β ,

TABLE 3. Selected bond distances (Å) for Na-, K-, and Ba-birnessite

	Na-birnessite	K-birnessite	Ba-birnessite
Mn-O1	1.931(4)	1.977(5)	1.961(5)
-O1	1.972(0)	1.978(7)	1.976(3)
-O1	1.882(2)	1.842(0)	1.847(4)
O1-O1	2.595(2)	2.657(9)	2.604(2)
-O1	2.413(0)	2.438(2)	2.532(5)
-O1	2.547(9)	2.847(6)	2.847(4)
-O1	2.851(0)	2.551(0)	2.436(6)
-O1	2.957(5)	2.943(2)	2.953(8)
-O1	2.953(6)	2.930(4)	2.949(6)
O1-O _{int}	2.590(9)	2.661(4)	2.634(6)
-O _{int}	2.795(9)	2.885(0)	2.809(8)
O _{int} -O _{int}	2.850(9)	2.847(6)	2.847(4)
O _{int} -O _{int}	2.953(6)	2.943(2)	2.953(8)
O _{int} -O _{int}	2.957(5)	2.930(4)	2.949(6)
	2.911(3)		

Note: O_{int} represents both the interlayer cation and the H₂O molecules.

and V. Ba²⁺, with an ionic radius of 1.49 Å (Shannon 1976) and a hydration radius of 4.0 Å (Nightingale 1959), nevertheless induced a unit-cell contraction after replacing Na⁺. The greater charge of Ba²⁺ leads to stronger bonding with the negatively charged Mn-O layers, resulting in a diminished interlayer spacing despite the larger hydration radius for Ba²⁺ and its halved occupancy relative to the starting Na.

The contraction of the interlayer region does not entail a decrease in primary bond lengths (Fig. 7). The O-H...O1 distances changed little following cation exchange, but the angles between octahedral layer oxygen ions and the interlayer oxygen decreased after both Ba- and K-exchange. Specifically, the O1-O1-O_{int} bond angles diminished from 93.5° in Na-birnessite to 87.7° in Ba-birnessite and 72.9° in K-birnessite (Fig. 7). Thus, the contraction of the unit cell following Ba- and K-exchange is effected by a change in bond angles that, in turn, reflect a re-arrangement of the interlayer cations, as described below.

Arrangement of interlayer species

According to Manceau et al. (1992), if there are no vacancies in the octahedral sheets, then the two-dimensional superperiodicity depends on the position of negative charge in the Mn-O sheet and the exchangeable cation valence. When the sheets do contain vacancies, they postulated that divalent cations will be situated above and below the vacancies, irrespective of layer charge. Our Rietveld refinement of the Mn occupancies in all of our samples yielded values close to 1.00, indicating that there were no vacancies in the Mn-O layer of the synthetic Na-, K-, and Ba-birnessite used in our study. Therefore, the interlayer hydrated cation positions most likely occurred adjacent to the Mn³⁺ sites in the Mn-O octahedral sheets, rather than near vacancies.

The interlayer atom positions used for initial refinement of the interlayer were determined from DELF maps. For these refinements, Na, K, Ba, and O(H₂O) were modeled as a single atomic species (oxygen, O_{int}). The combined effects of partial occupancies, positional disorder, and similarities in X-ray scattering factors for Na, K, and O rendered it impossible to distinguish among these species during the refinement. For clarification of the end-member structures, we modeled the interlayer O site with separate O (water) and cation sites, both constrained to occupy

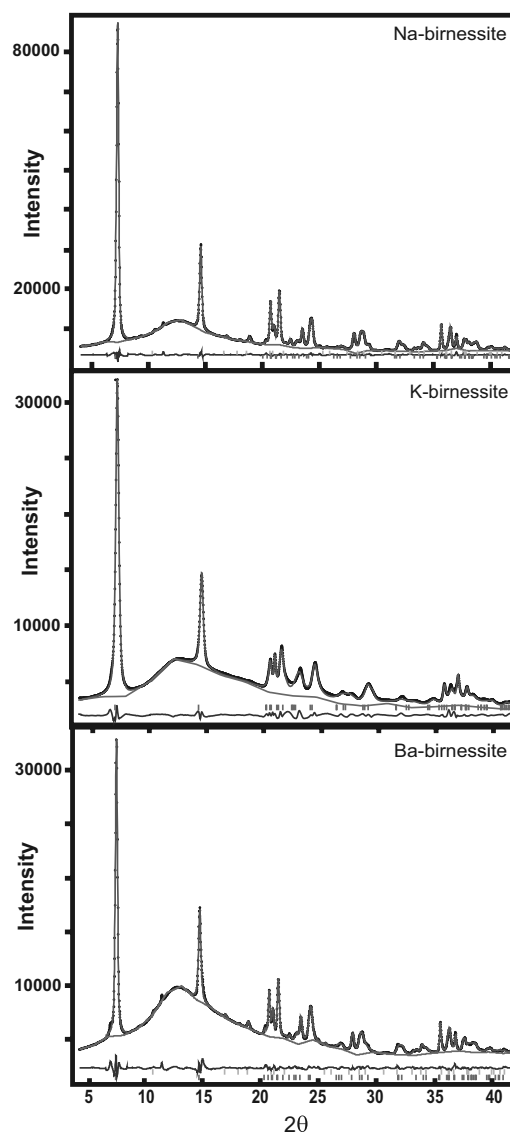


FIGURE 4. Observed (crosses), calculated (solid line), and difference (line below) plots for the end-member XRD patterns from 4.0 to 42.5 °2θ for: (a) Na-birnessite; (b) K-birnessite; and (c) Ba-birnessite. All were refined in a triclinic unit cell (C₁). Peak positions are indicated by vertical dashes.

the same position. The occupancy factors for the cations were fixed to the values determined by chemical analyses in Post and Veblen (1990), and the O (water) occupancy factor was refined (Table 2). As in Post et al. (2002), the split site for Na-birnessite is best described as two maxima separated by ~1 Å; therefore, both positions of the binary site are never occupied at the same time. The splitting of the interlayer sites is most likely caused by positional disorder of the Na⁺, Ba²⁺, and K⁺ cations, and H₂O molecules, such that they occupy different positions in the interlayer region in different unit cells. Therefore, the diffuse split sites apparent in the DELF maps must represent a composite average location for the interlayer species in the unit cell.

Again, as was found in Post et al. (2002) for Na-birnessite, the

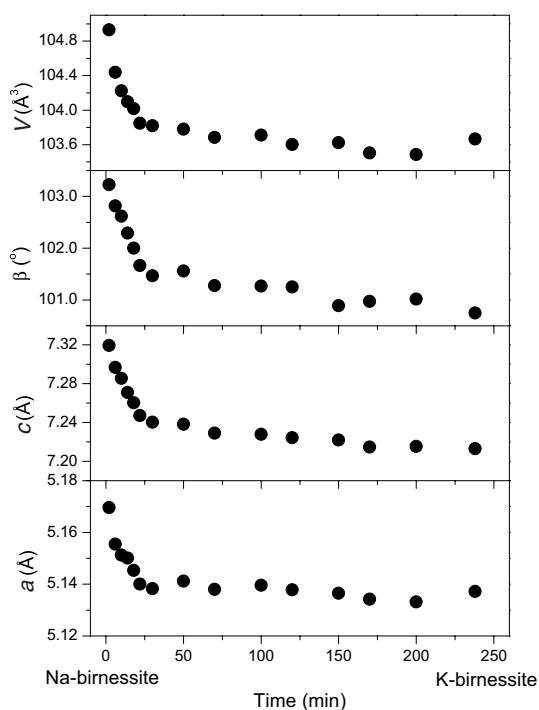


FIGURE 5. Changes in unit-cell parameters over time for the 0.01 *M* K-exchange reaction with Na-birnessite. The b , α , and γ parameters remained constant with exchange. The error bars calculated in GSAS are smaller than the plotting symbols.

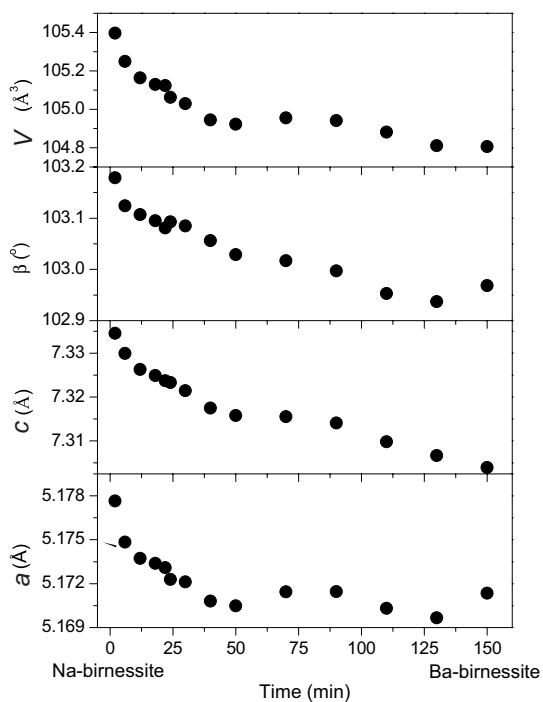


FIGURE 6. Changes in unit-cell parameters over time for the 0.01 *M* Ba-exchange reaction with Na-birnessite. The b , α , and γ parameters remained constant with exchange. The error bars calculated in GSAS are smaller than the plotting symbols.

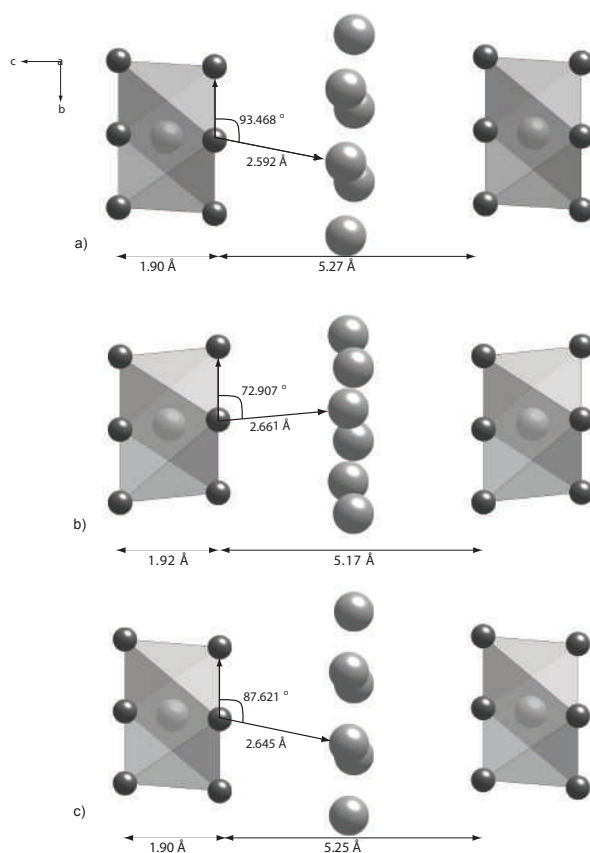


FIGURE 7. Diagrams revealing the angular relationships between the octahedral O atoms and the interlayer water species in the end-member birnessite phases as viewed down the a -axis. (a) Na-birnessite, (b) K-birnessite, (c) Ba-birnessite.

interlayer sites for Na-, K-, and Ba-birnessite form a hexagonal planar array parallel to the octahedral layers (Figs. 8 and 9). Each interlayer cation or H₂O molecule is surrounded by six other H₂O molecules with bond distances ranging from 2.85 to 2.95 Å (Table 3). The distances between octahedral O1 and interlayer O_{int} sites refined consistently to between 2.59 and 2.65 Å (Table 3), which might suggest H-bonds or, in the case of Na-birnessite, Na-O bonds (Post et al. 2002) between the octahedral oxygen and interlayer species. When Na is placed on a centroid between the split sites (an inversion center), bond distances are on the order of 2.9 to 3.0 Å, which are far from optimal. Based on the ionic radii presented in Shannon (1976), ^{vii}Na-^{iv}O bond distances ideally are 2.56 Å, as is consistent with Na-O bond distances observed in Na-rich aluminosilicates, such as albite (Harlow and Brown 1980). Nevertheless, our calculated Na-birnessite bond distances are very similar to those found both in Post et al. (2002) and Lanson et al. (2002), supporting the results of our refinement. The longer bond distances measured in these studies of birnessite may account for the extremely high susceptibility of interlayer Na to exchange for other cations.

Ideal ^{vii}Ba-^{iv}O distances are 2.76 Å (Shannon 1976), and when Ba²⁺ is placed on the centroid between split sites, a bond distance of 2.97 Å results. On the other hand, when Ba is situated on the lobes of the electron density ellipsoids in DELF syntheses,

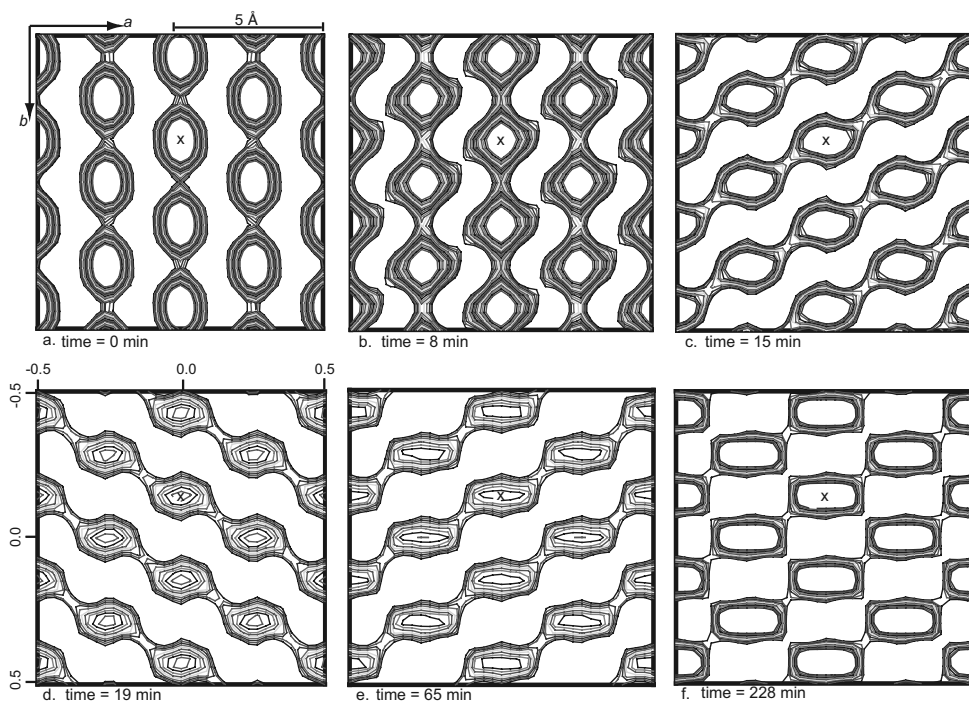


FIGURE 8. Difference electron Fourier (DELF) maps of the interlayer region calculated by GSAS for 0.01 *M* K-exchange reactions with Na-birnessite, for exchange times of (a) 0 min; (b) 8 min; (c) 15 min; (d) 19 min; (e) 65 min; and (f) 228 min. Areas of maximum electron density are located at the positions marked with an x. The contour interval is $0.1 e^{-}/\text{\AA}^3$. Elongation of the areas of electron density represents positional disorder of the interlayer cation and water species.

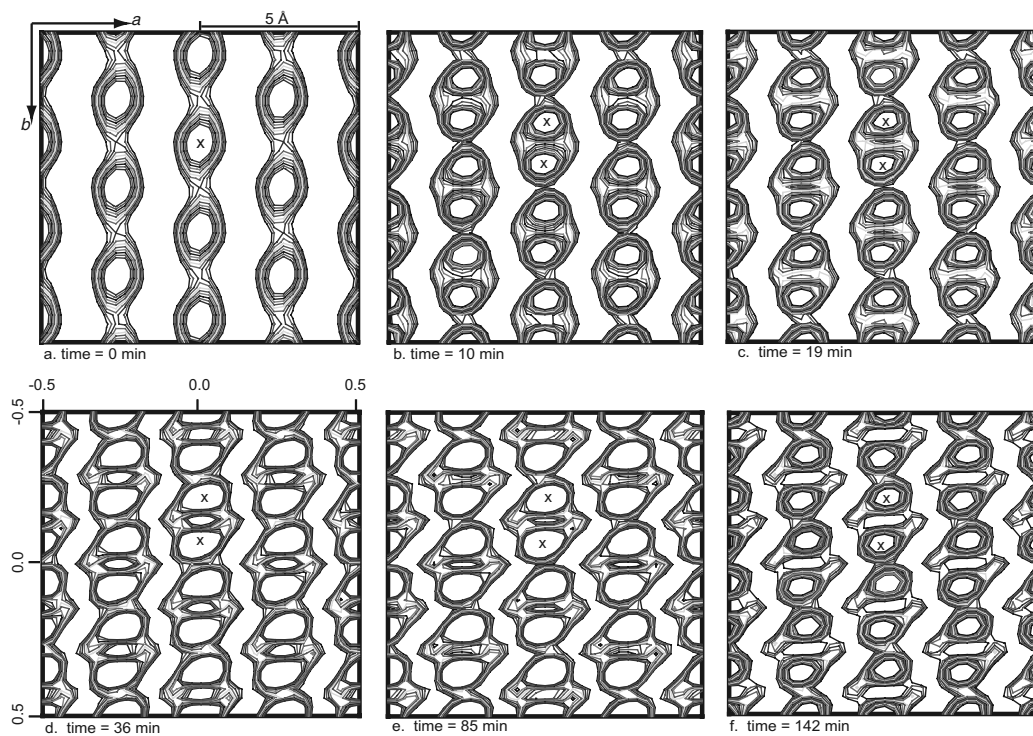


FIGURE 9. Difference electron Fourier (DELF) maps of the interlayer region calculated by GSAS for 0.01 *M* Ba-exchange reactions with Na-birnessite, for exchange times of (a) 0 min; (b) 10 min; (c) 19 min; (d) 36 min; (e) 85 min; and (f) 142 min. Areas of maximum electron density are located at the positions marked with an x. The contour interval is $0.1 e^{-}/\text{\AA}^3$. Splitting of the areas of electron density represents positional disorder of the Ba^{2+} and water species.

a Ba-O distance of 2.65 Å is observed (Table 3). Consequently, when Ba²⁺ substitutes into the interlayer, it is more likely to be located toward the lobes of the split site as opposed to the centroid. In contrast, the ideal ^{VII}K-^{VI}O ideal bond distance is 2.89 Å (Shannon 1976), and when K⁺ is placed on the centroid in the interlayer, its bond distances to the interlayer oxygen atoms are 2.85 Å. When K⁺ is situated on the lobes of the DELF ellipsoids, the corresponding K-O distances are 2.66 Å (Table 3). Therefore, we infer that K⁺ is located on the centroid of the split sites when it substitutes into the interlayer. When H₂O occupies that site, the O atom is sited on the lobe to achieve an O-H...O bond distance of 2.66 Å, as is characteristic of hydrogen bonds. Thus, our refinement suggests that both the positional disorder and the variability in the interlayer configurations of Na-, K-, and Ba-birnessite are explainable to a large degree by optimization of bond distances.

Real-time analyses

Difference maps for 00*l* sections near $z = 0.5$ revealed systematic and continuous changes in the positions of the interlayer species as the reactions progressed (Figs. 8 and 9). Split electron-density maxima with centroids at (0 0 0.5) are present in electron difference maps for Na, K, and Ba end-members; however, with increased substitution of K⁺ for Na⁺, the axis connecting the split-site maxima rotated from an orientation parallel to the *b*-axis to an orientation parallel to *a*. The split electron density maxima of interlayer Ba²⁺, on the other hand, exhibited no rotation, but the degree of splitting grew more pronounced. Thus, our real-time XRD results suggest that the transition from one interlayer configuration to another as cationic substitution proceeds involves continuous shifts in atomic positions rather than the co-existence of end-member configurations. This interpretation runs counter to arguments that exchange processes occur through dissolution of one phase and precipitation of another (e.g., Putnis 2002). Nevertheless, we note that the gradual evolution reported here also represents structures that are averaged over many unit cells, as is inherent to the XRD process.

Although the shifting in interlayer positions is gradual, the kinetics of substitution occurs as a two-step process. The first and more rapid stage involves a repositioning that may correspond with exchange of the interlayer species, and the second slower step entails an ordering of the interlayer species into those new positions. For example, the 90° rotation of the ellipsoid that represents interlayer positional disorder in Na-birnessite was completed within 20 min of exchange with K. Since the interlayer species controls the evolution of the unit-cell parameters, the decrease in unit-cell volume followed a similar behavior. Initially, the decrease in unit-cell volume was rapid, generally within 15 to 20 minutes after the initiation of fluid flow. The subsequent stage involved a smaller variation in unit-cell parameters. We have determined that for K-exchange the initial stage had a coefficient of unit-cell contraction of -8.96×10^{-6} 1/s, and the second stage had a contraction coefficient of -2.66×10^{-7} 1/s. Ba-exchange resulted in a contraction coefficient of -2.17×10^{-6} 1/s for the initial stage (the first 15–20 min) and -2.71×10^{-7} 1/s for the second stage. Ongoing research into the kinetics of these reactions in combination with molecular dynamical modeling will further elucidate the cation exchange processes in birnessite.

ACKNOWLEDGMENTS

Funding for this research was provided by NSF grants EAR01-25908 and EAR04-17741 and by a Penn State Materials Research Institute (MRI) SEED grant. We are grateful for the comments of two anonymous reviewers. Thanks go to YongJae Lee of the Brookhaven National Lab for his assistance with the operation of the environmental cell. This research was carried out at the National Synchrotron Light Source, Brookhaven National Laboratory, which is supported by the U.S. Department of Energy, Division of Materials Sciences and Division of Chemical Sciences, under contract no. DE-AC02-98CH10886.

REFERENCES CITED

- Banerjee, D. and Nesbitt, H.W. (1999) Oxidation of aqueous Cr(III) at birnessite surfaces: constraints on reaction mechanism. *Geochimica et Cosmochimica Acta*, 63, 1671–1687.
- Burns, R.G. and Burns, V.M. (1976) Mineralogy of ferromanganese nodules. In G.P. Glasby, Ed., *Marine Manganese Deposits*, p. 185–248. Elsevier, Amsterdam.
- Cornell, R.M. and Giovanoli, R. (1988) Transformation of hausmannite into birnessite in alkaline media. *Clays and Clay Minerals*, 36, 249–257.
- Dixon, J.B., Golden, D.C., Uzochukwu, G.A., and Chen, C.C. (1986) Soil Manganese Oxides. In M.H.B. Hayes and A. Herbillon, Eds., *Soil Colloids, Structures and Associations in Soil Aggregates*. NATO Workshop, Ghent, Belgium.
- Feng, Q., Kanoh, H., and Ooi, K. (1999) Manganese oxide porous crystals. *Journal of Materials Chemistry*, 9, 319–333.
- Finger, L.W., Cox, D.E., and Jephcoat, A.P. (1994) A correction for powder diffraction peak asymmetry due to axial divergence. *Journal of Applied Crystallography*, 27, 892–900.
- Golden, D.C., Chen, C.C., and Dixon, J.B. (1986) Synthesis of todorokite. *Science*, 231, 717–719.
- — — (1987) Transformation of birnessite to busserite, todorokite, and manganite under mild hydrothermal treatment. *Clays and Clay Minerals*, 35, 271–280.
- Hammersley, A.P., Svensson, S.O., Hanfland, M., Fitch, A.N., and Hausermann, D. (1996) Two-dimensional detector software: From real detector to idealized image or two-theta scan. *High Pressure Research*, 14, 235–248.
- Harlow, G.E. and Brown, G.E. (1980) Low albite: an X-ray and neutron diffraction study. *American Mineralogist*, 65, 986–995.
- Kuma, K., Usui, A., Paplawsky, W., Gedulin, B., and Arrhenius, G. (1994) Crystal structures of synthetic 7 and 10 Å manganates substituted by mono-valent cations. *Mineralogical Magazine*, 58, 425–447.
- Lanson, B., Drits, V.A., Feng, Q., and Manceau, A. (2002a) Structure of synthetic Na-birnessite: Evidence for a triclinic one-layer unit-cell. *American Mineralogist*, 87, 1662–1671.
- Lanson, B., Drits, V.A., Gaillot, A., Silvester, E., Plançon, A., and Manceau, A. (2002b) Structure of heavy-metal sorbed birnessite: Part I. Results from X-ray diffraction. *American Mineralogist*, 87, 1631–1645.
- Larson, A.C. and Von Dreele, R.B. (2006) GSAS-General Structure Analysis System. Los Alamos National Laboratory Report No. LAUR 86-748.
- Lee, Y., Carr, S.W., and Parise, J.B. (1998) Phase transition upon K⁺ ion exchange into Na-low silica X: combined NMR and synchrotron x-ray powder diffraction study. *Chemistry of Materials*, 10, 2561–2570.
- Lee, Y., Kim, S., Schoonen, M.A.A., and Parise, J.B. (2000) Structural and Sr²⁺ ion exchange studies of gallosilicate TsG-1. *Chemistry of Materials*, 12, 1597–1603.
- Leroux, F., LaSalle, A.L., Guyomard, D., and Piffard, Y. (2001) Interleaved oxovanadium cations in the rancieite manganese oxide delta-MnO₂. *Journal of Materials Chemistry*, 11, 652–656.
- Luo, J. and Suib, S.L. (1997) Preparative parameters, magnesium effects and anion effects in the crystallization of birnessites. *Journal of Physical Chemistry B*, 101, 10403–10413.
- Luo, J., Huang, A., Park, S.H., Suib, S.L., and O'Young, C. (1998) Crystallization of sodium-birnessite and accompanied phase transformation. *Chemistry of Materials*, 10, 1561–1568.
- Luo, J., Zhang, Q., and Suib, S.L. (2000) Mechanistic and kinetic studies of crystallization of birnessite. *Inorganic Chemistry*, 39, 741–747.
- Ma, Y., Luo, J., and Suib, S.L. (1999) Synthesis of birnessites using alcohols as reducing reagents: Effects of synthesis parameters on the formation of birnessites. *Chemistry of Materials*, 11, 1972–1979.
- Manceau, A., Charlet, L., Boisset, M.C., Didier, B., and Spadini, L. (1992) Sorption and speciation of heavy metals on hydrous Fe and Mn oxides. From microscopic to macroscopic. *Applied Clay Science*, 7, 201–223.
- McKenzie, R.M. (1971) The synthesis of birnessite, cryptomelane, and some other oxides and hydroxides of manganese. *Mineralogical Magazine*, 38, 493–502.
- Nightingale, E.R. (1959) Phenomenological theory of ion solvation. Effective radii of hydrated ions. *Journal of Physical Chemistry*, 63, 1381–1387.
- Parise, J.B., Cahill, C.L., and Lee, Y. (2000) Dynamic powder crystallography with synchrotron X-ray sources. *Canadian Mineralogist*, 38, 777–800.
- Paterson, E., Clarke, D.R., Russell, J.D., and Swaffield, R. (1986) Cation exchange in synthetic manganates II. The structure of an alkylammonium-saturated phyllo-manganate. *Clay Minerals*, 21, 957–964.
- Post, J.E. (1992) Crystal structures of manganese oxide minerals. *Catena Supple-*

- ment, 21, In H.C.W. Skinner and R.W. Fitzpatrick, Eds., *Biominalization, processes of iron and manganese*, Catena Supplement 21, p. 51–73. Catena Verlag, Germany.
- — — (1999) Manganese oxide minerals: Crystal structures and economic and environmental significance. In J.V. Smith, Ed., *Colloquium on Geology, Mineralogy, and Human Welfare*, 91, p. 3447–3454. Proceedings of the National Academy of Sciences, Washington, D.C.
- Post, J.E. and Bish, D.L. (1989) Rietveld refinement of crystal-structures using powder X-ray diffraction data. In D.L. Bish and J.E. Post, Eds., *Modern Powder Diffraction*, 20, p. 277–308. Reviews in Mineralogy, Mineralogical Society of America, Chantilly, Virginia.
- Post, J.E. and Veblen, D.R. (1990) Crystal structure determinations of synthetic sodium, magnesium, and potassium birnessite using TEM and the Rietveld method. *American Mineralogist*, 75, 477–489.
- Post, J.E., Heaney, P.J., and Hanson, J. (2002) Rietveld refinement of a triclinic structure for synthetic Na-birnessite using synchrotron powder diffraction data. *Powder Diffraction*, 17, 218–221.
- Putnis, A. (2002) Mineral replacement reactions: From macroscopic observations to microscopic mechanisms. *Mineralogical Magazine*, 66, 689–708.
- Rietveld, H.M. (1969) A profile refinement method for nuclear and magnetic structures. *Journal of Applied Crystallography*, 2, 65–71.
- Shannon, R.D. (1976) Revised effective ionic radii and systematic studies of interatomic distances in halides and chalcogenides. *Acta Crystallographica A*, 32, 751–767.
- Shen, Y.F., Zerger, R.P., DeGuzman, R.N., McCurdy, L., Potter, D.I., and O'Young, C.L. (1993) Manganese oxide octahedral molecular sieves: Preparation, characterization, and applications. *Science*, 260, 511–515.
- Stephens, P.W. (1999) Phenomenological model of anisotropic peak broadening in powder diffraction. *Journal of Applied Crystallography*, 32, 281–289.
- Thompson, P., Cox, D.E., and Hastings, J.B. (1987) Rietveld refinement of Debye-Scherrer synchrotron X-ray data from Al_2O_3 . *Journal of Applied Crystallography*, 20, 79–83.
- Toby, B.H. (2001) EXPGUI, a graphical user interface for GSAS. *Journal of Applied Crystallography*, 34, 210–213.

MANUSCRIPT RECEIVED FEBRUARY 17, 2006

MANUSCRIPT ACCEPTED SEPTEMBER 25, 2006

MANUSCRIPT HANDLED BY HONGWU XU